Proceedings of the ASME 2023 43rd International Conference on Ocean, Offshore Arctic Engineering
OMAE 2024
June 9-14, 2024, Singapore EXPO, Singapore

OMAE2024-126338

NUMERICAL VALIDATION OF SECOND-ORDER WAVE DRIFT FORCES CALCULATION FOR FLOATING STRUCTURES

Krishnavelu Ramachandran[1,†,*], Abhilash Somayajula[1,†,*]

[1]Marine Autonomous Vehicles (MAV) Laboratory
Department of Ocean Engineering, Indian Institute of Technology Madras
Chennai - 600 036, Tamil Nadu, India

ABSTRACT

Accurate estimation of second-order wave drift forces is imperative for predicting the responses of offshore structures, mooring systems, and vessel motions in ocean waves, especially in adverse wave conditions. These wave drift forces are derived from non-linear wave potential effects. Precise estimation of wave drift forces is vital for the design and analysis of offshore platforms, moored structures, and ships operating in challenging wave conditions to ensure safety, stability, fatigue resistance, and long-term structural integrity. This study presents a comprehensive derivation and implementation of second-order wave drift forces for an in-house numerical tool, Hydrodynamic Response Analysis (HydRA). The HydRA program has been developed using a Green function-based 3-D potential flow theory-based panel method code. The numerical investigation focuses on the Benchmark KRISO Container ship (KCS) for this study. The HydRA tool accurately calculates wave drift forces at zero speed case. This numerical simulation tool is capable of accurately assessing rigid body motions and loads in all six degrees of freedom. Validation of the second-order drift forces at zero speed will be conducted against the MDLHydroD and WAMIT programs. This research contributes to the advancement of understanding and predicting second-order wave drift forces, offering valuable insights into the field of fluid-structure interaction and hydrodynamics analysis.

Keywords: HydRA, Second-order wave drift forces, Mean wave drift forces, Added Resistance, Potential flow theory, 3D-Panel method code, MDLHydroD, Hydrodynamics, KCS, KVLCC2, Fluid-Structure interaction.

[†]Joint first authors
[*]Corresponding author: abhilash@iitm.ac.in, oe20d014@smail.iitm.ac.in, krishnavelgce@gmail.com

1. INTRODUCTION

A precise understanding of low-frequency wave drift forces is vital for capturing the intricate loads acting on floating bodies. Traditionally, the perturbation method solves the hydrodynamic problem of these bodies in the ocean. Nonlinear forces from ocean waves become pronounced when both the waves and induced motions have larger amplitudes. Despite their significance, these effects are often overlooked in initial structural design due to complexity and incomplete understanding. Mathematically, this nonlinear problem is segmented into first-order, second-order, and higher-order components. The first-order force is estimated from velocity potential and wave elevation obtained by solving the linearized boundary value problem governed by the Laplace equation. Subsequently, the solution guides the estimation of second-order wave drift forces, categorized into difference frequency and sum frequency components in frequency domain analysis. For bi-chromatic waves with components of the same frequency, the difference frequency component is a steady force. Conversely, in general bi-chromatic waves, both components exhibit harmonic variations over time due to interactions with various frequency pairs. Slowly varying wave drift forces in real seas originate from difference frequency interactions among wave components [1]. These second-order forces, particularly the effects of difference and sum frequencies, are crucial for addressing challenges in floating structures' dynamic behavior, including those in wind turbines, offshore structures, and ships.

Simulation tools based on potential flow theory are increasingly used to estimate added resistance, wave-induced forces, and moments in fluid-structure interaction problems, crucial for large structures. Specifically, for ship-shaped structures like FPSOs, inherent frequencies lie beyond typical wave ranges [2]. Furthermore, numerical simulations that aim to capture the maneuvering behavior of a ship in waves must include second-order mean wave drift forces and moments.

First and second-order wave forces, derived from linear potential flow theory, are crucially estimated for accurate predictions. The Quadratic Transfer Function (QTF) describes second-order forces and moments. Superposing velocity potential is vital for precision. Huijsmans et al.[3] outlined constructing a uniform expansion of the speed-dependent wave potential. Ramery et al.[4] and Hermans et al.[5] addressed precise assessments for effective characterization of ship motion, including drift forces and wave drift damping coefficients.

Typically, two primary methods, the Near-field and Far-field, assess added resistance and mean wave drift forces. Far-field analyzes diffracted and radiated wave energy at infinity, while Near-field provides accessible understanding, advantageous for multiple bodies. Pinkster et al.[6] introduced Near-field, integrating pressure for up to second-order wave slope. Later, Pinkster et al.[7] provided a summary of the calculation for the second-order wave drift force. Maruo et al.[8] employed Far-field numerically, analyzing horizontal drift forces in various settings. Papanikolaou et al.[9] developed a 3D panel method for seakeeping analysis, incorporating near-field pressure integration to estimate second-order drift forces [10]. Liu et al.[11] developed a parallel panel method using the far field to assess mean wave drift forces. Fonseca et al.[1] computed second-order drift forces on FPSO structures across various wave frequency components using the near-field method, estimating forces and motions up to the second order. These efforts highlight the continuous refinement of computational tools for understanding vessel dynamics under wave-induced forces.

Second-order wave drift forces are determined in two conditions: zero speed and forward speed of the vessel. At zero speed, vessel to rest condition, the added resistance equals longitudinal drift force. Conversely, during forward motion, second-order forces counteract the forward movement. Somayajula and Falzarano [2] developed a SIMDYN simulation tool for time domain calculations, based on MDLHydroD program frequency domain mean drift forces developed by Guha and Falzarano [12]. They validated results against OrcaFlex software for KVLCC2 ship roll motion. Yasukawa et al.[13] analyzed ship maneuvering through experimental and numerical methods, employing the zero-speed 3D Panel method (3DPM) and strip theory-based Kochin-function method (SKFM) for wave-induced forces during forward motion. Fournarakis et al.[14] estimated drift forces, moments, and added resistance on the KVLCC2 tanker hull numerically, validating against experimental and CFD data. These studies emphasize the importance of accurately predicting wave-induced forces for vessel performance assessment in various conditions.

This study utilized the "MDLHydroD" simulation tool, a 3D Green function panel code based potential flow theory in the frequency domain, to validate our numerical results. Developed by Guha [15], the comprehensive implementation details of this in-house program are outlined in reports by Guha [15, 16]. This program is capable of calculating wave drift forces and moments under both zero-speed and forward-speed conditions and has been instrumental in various studies validating numerical outcomes [2, 12, 17–19]. Furthermore, Krishnavelu et al.[20] conducted an in-depth analysis, comparing experimental and simulation studies on ship maneuvering in waves. This simulation tool was used to estimate second-order mean wave drift forces and moments. subsequently, these forces were added with a mathematical model to simulate vessel maneuvering motions in regular waves.

This study introduces a Hydrodynamic Response Analysis - "HydRA" program, an in-house numerical simulation program has been developed based on a potential theory-based 6-DOF 3D Green function panel method code for estimating the Hydrodynamic Response Analysis of a floating structure. The simulation program exhibits the capability to compute wave forces at zero-speed case in either the frequency or time domain. This paper describes the theoretical foundation and numerical implementation of calculating the second-order wave drift force and motions. This study focuses on the Benchmark KRISO Container ship (KCS) with subsequent validation against the MDLHydroD and WAMIT program.

2. POTENTIAL FLOW THEORY

The theoretical potential flow theory has been used to solve the external flows around the body. The velocity function $\phi(x, y, z, t)$ is a continuous function that satisfies the conservation of mass described by the Laplace equation. It assumes that the fluid is incompressible, inviscid, and irrotational flow. This section explains the coordinate system, governing equation, and boundary conditions detailed for solving the physics of the fluid flow. In this study, The mathematical derivation for wave drift forces calculation is based on the works of Somayajula and Falzarano [2], Guha [16], and Journée, and Massie [21].

2.1 Coordinate system

In this study, there are three coordinate axes systems considered to represent the floating body kinematics and responses for all six degrees of freedom which is shown in Figure 1. The right-handed East, North, Up (ENU) coordinate axes are listed below:

- **1**. **Global fixed coordinate system (GCS)**: This coordinate system is always fixed to the earth's surface in the origin. which is represent as a $O_0 = (X_0, Y_0, Z_0)$. This fixed system is commonly known as an inertial coordinate system.

- **2**. **Steady moving coordinate system (SMCS)**: A floating body or vessel is moving at a steady constant speed in the x-direction then the resultant velocity is represented as ($U = U\hat{i} + 0\hat{j} + 0\hat{k}$). This system coordinates axes at the origin of the body $O = (X, Y, Z)$. It is also called an inertial axes system.

- **3**. **Body fixed coordinate system (BCS)**: This coordinate system is always attached to the body at the origin $O' = (X', Y', Z')$. The BCS coordinate axes always coincide with the SMBC coordinate axes when the body is at rest condition but these axes are different when the body translates or rotates due to the presence of incident waves or any other external forces.

The Figure 1 shows that a unit frequency wave ω_I acting on the body at certain drift angle β. The drift angle is an angle

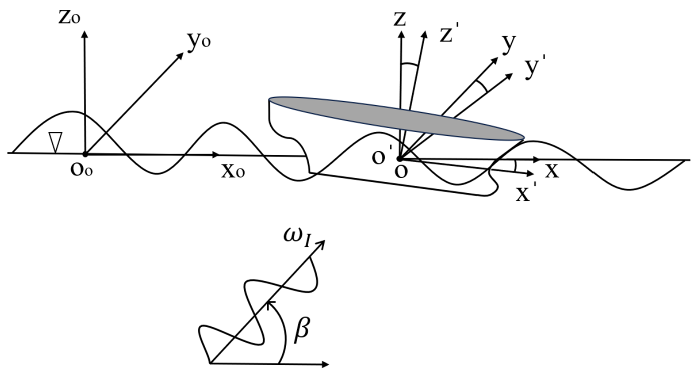

FIGURE 1: THREE COORDINATE SYSTEMS

between the incident wave to the longitudinal axes of the GCS frame in the anticlockwise direction. When the vessel moves with a steady forward speed U which encounters the incident wave then the frequency of the wave changes due to the Doppler effect. The varying frequency is called a encountering wave frequency (ω_e). The encountering wave frequency is expressed in the equation (1) as a function of a ship forward steady speed U, incident wave frequency w_I, wave number k_I, and drift angle β.

$$\omega_e = \omega_I - k_I U cos\beta \tag{1}$$

The wave number k_I is expressed as:

$$k_I = \frac{\omega_I^2}{g} \tag{2}$$

2.2 Velocity potential and Boundary conditions

A linear boundary value problem can be defined under the assumption of small amplitude wave motion to determine the velocity potential of the flow. The SMCS frame allows the vessel to respond in all six degrees of freedom due to incident waves. When the vessel moves at a steady forward speed U, it experiences the same speed in negative x-direction which is shown in Figure 2. The complex velocity potential $\Phi(x,t)$ in the entire fluid domain is expressed as:

$$\Phi(x,t) = -Ux + \underbrace{\phi_{St}(x)}_{\text{neglected}} + \phi_I(x,\omega_I,\beta) + \phi_S(x,\omega_I,\beta) + \sum_{i=1}^{6} \xi_i \phi_i(x,\omega_e,\beta) \tag{3}$$

Where, ϕ_I is the incident wave potential, ϕ_S is the diffracted or scattered wave potential, ϕ_i is the rational potential due to the unit amplitude of the vessel motion, ϕ_{St} is a steady potential due to the motion of the body in straight. Due to the presence of the body, the steady flow around the hull neglects the effect of steady potential. This perturbation potential effect is insignificant at the moderate speed of the ship. It is simply neglected in the equation (3).

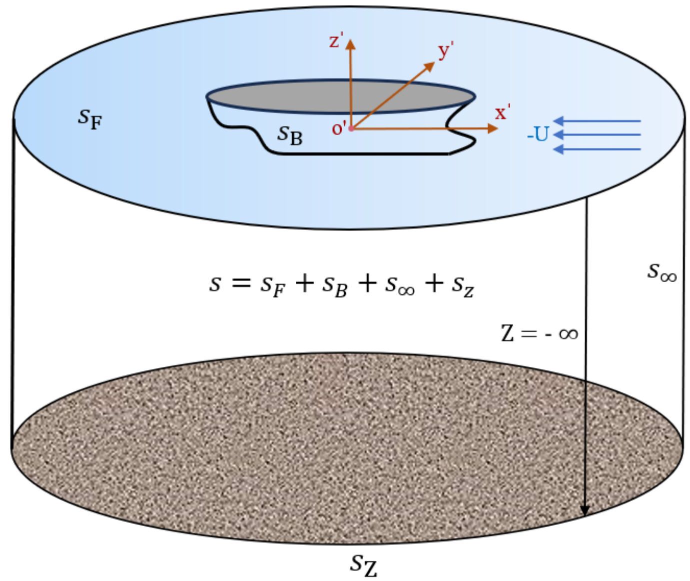

FIGURE 2: BOUNDARY CONDITIONS

Governing Equation: Laplace equation governs the spatial distribution of the velocity potential. The complex velocity potential must satisfy the Laplace equation. This equation captures essential aspects of the fluid's behavior throughout the entire fluid domain.

$$\nabla^2 \Phi(x,t) = 0 \tag{4}$$

Boundary Conditions: The Figure 2 shows the essential boundary conditions are needed to fully define the fluid flow by using velocity potential and ensure that the solution is physically realistic. The combination of the Laplace equation and the appropriate boundary conditions constitutes a complete set of equations for potential flow in the fluid domain. The boundary conditions are listed below:

1. **Bottom Boundary Condition (BBC):** The velocity of the fluid flow in the normal direction to the bottom is equal to the velocity of the sea-bottom boundary in the normal direction. The velocity is zero at the sea bed because the bottom does not allow the fluid to penetrate.

$$\omega = \frac{\partial \phi}{\partial z} = 0 \quad \text{over the bottom } z = -\infty \tag{5}$$

2. **Radiation Boundary Condition (RBC):** It is also referred to as Sommerfeld Boundary Condition (SBC). The response of the vessel generated radiation waves around the body due to the incident wave. These waves propagated horizontally over an infinite (∞) distance.

$$\lim_{r\to\infty} \sqrt{r}\left[\frac{\partial \phi_S}{\partial r} - ik\phi_S\right] = 0 \tag{6}$$

$$\lim_{r\to\infty} \sqrt{r}\left[\frac{\partial \phi_i}{\partial r} - ik\phi_i\right] = 0, i = 1,2,3,4,5,6 \tag{7}$$

3. **Body Boundary Condition (BBC):** The velocity of the fluid flow in the normal direction anywhere around the underwater body is equal to the normal velocity of the body boundary.

$$(V_S - \Delta\Phi)\,.\,\hat{n} = 0 \tag{8}$$

4. **Kinematic Free-surface Boundary Condition (KFSBC):** The velocity of the fluid in the normal direction of the free surface is equal to the normal velocity of the free surface. The free surface does not allow the water particles to escape or penetrate into the surface.

$$\frac{\partial \phi}{\partial t} = -\left(\frac{\partial \phi}{\partial z} - \left(-U + \frac{\partial \phi}{\partial x}\right)\frac{\partial \eta}{\partial x} - \frac{\partial \phi}{\partial y}\frac{\partial \eta}{\partial y}\right) \quad \text{over } z = \eta(x,y,t) \tag{9}$$

5. **Dynamic Free-surface Boundary Condition (DFSBC):** The unsteady Bernoulli's equation has been used to solve the velocity potential over the free surface. It assumes that the pressure on the free surface is constant $C = 0$.

$$\frac{\partial \phi}{\partial t} + \frac{1}{2}\left\{\left(-U + \frac{\partial \phi}{\partial x}\right)^2 + \left(\frac{\partial \phi}{\partial y}\right)^2 + \left(\frac{\partial \phi}{\partial z}\right)^2\right\} + g\eta = 0 \quad \text{over } z = \eta(t,x,y) \tag{10}$$

2.3 Perturbation method

The perturbation approach is a popular method for solving non-linear problems across varying degrees of non-linearity. The Kinematic free surface boundary condition and body boundary conditions are in a non-linear manner. It is difficult to solve the non-linear problem in a straightforward. The non-linear parameters are expressed linearly from the first order to the higher order such as velocity potential, wave elevation, pressure, normal vector, and position vector. Which means that all parameters are assumed to vary very slightly relative to the order of wave slope (ϵ).

$$\begin{aligned}
\phi &= \epsilon\phi^{(1)} + \epsilon^2\phi^{(2)} + \epsilon^3\phi^{(3)} + \dots \\
\eta &= \epsilon\eta^{(1)} + \epsilon^2\eta^{(2)} + \epsilon^3\eta^{(3)} + \dots \\
p &= p^{(0)} + \epsilon p^{(1)} + \epsilon^2 p^{(2)} + \epsilon^3 p^{(3)} + \dots \\
n &= n^{(0)} + \epsilon n^{(1)} + \epsilon^2 n^{(2)} + \epsilon^3 n^{(3)} + \dots \\
x &= x^{(0)} + \epsilon x^{(1)} + \epsilon^2 x^{(2)} + \epsilon^3 x^{(3)} + \dots
\end{aligned} \tag{11}$$

Where, ϵ is a small number ($\epsilon << 1$), which denotes the order of oscillation as a wave slope. $p^{(0)}$ is the Hydrostatic pressure.

The conversion of nonlinear boundary conditions into linearized forms is a key step in solving a sequence of Laplace equations systematically. Initiating this process, the first-order velocity potential ϕ^1 is derived by addressing the linearized problem. Subsequently, the solution obtained for first-order potential ϕ^1 serves as an input for computing the linearized problem associated with the second-order velocity potential ϕ^2 and so on. This iterative approach extends to higher orders. The Laplace equation and all boundary conditions are considered up to the first-order velocity potential. Those equations are rewritten based on the parameters up to first order which are expressed as:

$$\nabla^2\phi^{(1)} = 0 \tag{12}$$

$$\frac{\partial \eta^{(1)}}{\partial t} - U\frac{\partial \eta^{(1)}}{\partial x} = \frac{\partial \phi^{(1)}}{\partial z} \quad \text{over } z = 0 \tag{13}$$

$$\frac{\partial \phi^{(1)}}{\partial t} - U\frac{\partial \phi^{(1)}}{\partial x} = -g\eta^{(1)} \quad \text{over } z = 0 \tag{14}$$

$$\frac{\partial \phi^{(1)}}{\partial n} = \sum_{k=1}^{6} \dot{\xi}_k n_k + \xi_k m_k \quad \text{over } S_0 \tag{15}$$

$$\frac{\partial \phi^{(1)}}{\partial z} = 0 \quad \text{over } z = -\infty \tag{16}$$

where, S_0 is the mean underwater hull surface.

3. SECOND ORDER WAVE FORCES AND MOMENTS

This study analyzed second-order wave drift forces and moments acting on the body in forward speed based on the direct pressure integration over the instantaneous wetted surface of the hull. The numerical derivation for the calculation of the wave forces and moments are represented in this section.

3.1 Pressure calculation

The unsteady Bernoulli's equation is used to calculate the pressure over the wetted body surface S. The pressure term will become zero in the equation because the pressure on the free surface is assumed as constant C = 0.

The pressure at any point within the fluid is determined using the unsteady Bernoulli's equation is expressed as:

$$\begin{aligned}
p &= -\rho g z - \rho\frac{\partial \Phi}{\partial t} - \frac{\rho}{2}|\Delta\Phi|^2 \\
&= -\rho g z - \rho\frac{\partial \phi}{\partial t} + \rho U\frac{\partial \phi}{\partial x} \underbrace{-\frac{\rho U^2}{2}}_{\text{neglected}} \\
&\quad - \frac{\rho}{2}\left\{\left(\frac{\partial \phi}{\partial x}\right)^2 + \left(\frac{\partial \phi}{\partial y}\right)^2 + \left(\frac{\partial \phi}{\partial z}\right)^2\right\}
\end{aligned} \tag{17}$$

The terms denoting constant gauge pressure, specifically $-\frac{\rho U^2}{2}$, can be excluded from the above dynamic pressure equation.

$$\begin{aligned}
p &= -\rho g z - \rho\frac{\partial \phi}{\partial t} + \rho U\frac{\partial \phi}{\partial x} \\
&\quad - \frac{\rho}{2}\left\{\left(\frac{\partial \phi}{\partial x}\right)^2 + \left(\frac{\partial \phi}{\partial y}\right)^2 + \left(\frac{\partial \phi}{\partial z}\right)^2\right\}
\end{aligned} \tag{18}$$

The total pressure acting on the fluid is expressed as a sum of terms which is expressed in the equation (11) such as hydrostatic pressure, first-order pressure, second-order pressure, and so on. The hydrodynamic forces and moments acting on the body are obtained by integrating the pressure over the wetted surface area of the vessel.

$$F = \int_S p \cdot \hat{n}\, dS \tag{19}$$

$$M = \int_S p \cdot (x \times \hat{n})\, dS \tag{20}$$

The above force and moment equations are also expressed by the perturbation method like a pressure expression.

$$F = F^{(0)} + \epsilon^{(1)} F^{(1)} + \epsilon^{(2)} F^{(2)} + \ldots \tag{21}$$

$$M = M^{(0)} + \epsilon^{(1)} M^{(1)} + \epsilon^{(2)} M^{(2)} + \ldots \tag{22}$$

3.2 Hydrodynamic Force and Moment calculation

The wetted surface area of the body S is not constant over the period. This surface S is instantaneously changing due to the variation of the wave elevation. The total wetted surface area of the body is shown in Figure 3. which is divided into two parts: one for constant (S_0) part up to the constant draft level of the body. Another part is an oscillating water level s which represents the splash zone between the static waterline and the wave profile along the body. It is important to represent accurately to calculate the wave drift forces and moment acting on the body.

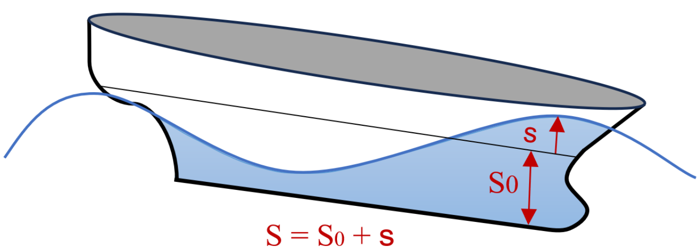

FIGURE 3: BODY WETTED SURFACE

The hydrodynamic forces and moments are expressed as following equations:

$$\begin{aligned} F = &\left(\int_{S_0} dS + \epsilon \int_s \zeta_r ds + \ldots\right) \\ &\left\{p^{(0)} + \epsilon^{(1)} p^{(1)} + \epsilon^{(2)} p^{(2)} + \ldots\right\}. \\ &\left\{\hat{n}' + \epsilon\left(\theta^{(1)} \times \hat{n}'\right) + \epsilon^{(2)} H\hat{n}' + \ldots\right\} \end{aligned} \tag{23}$$

$$\begin{aligned} M = &\left(\int_{S_0} dS + \epsilon \int_s \zeta_r ds + \ldots\right) \\ &\left\{p^{(0)} + \epsilon^{(1)} p^{(1)} + \epsilon^{(2)} p^{(2)} + \ldots\right\}. \\ &\left\{(x' \times \hat{n}') + \epsilon\left[\xi^{(1)} \times \hat{n}' + \theta^{(1)} \times (x' \times \hat{n}')\right]\right. \\ &\left. + \epsilon^{(2)}\left[H(x' \times \hat{n}') + \xi^{(1)} \times (\theta^{(1)} \times \hat{n}')\right] + \ldots\right. \end{aligned} \tag{24}$$

where,

$\int_s \zeta_r ds$ is the waterline surface integral due to the Taylor expansion of the integral on the instantaneous fully wetted surface area S concerning the draft waterline surface S_0. This waterline surface integral is either positive or negative.

ζ_r is the relative waterline which is expressed as:

$$\zeta_r = \eta - (\xi_3 - \xi_5 x + \xi_4 y) \tag{25}$$

$\xi^{(1)}$ is the first order displacement which is expressed as:

$$\xi^{(1)} = \xi_1 \hat{i} + \xi_2 \hat{j} + \xi_3 \hat{k} \tag{26}$$

$\theta^{(1)}$ is the first-order rotation vector which is expressed as:

$$\theta^{(1)} = \xi_4 \hat{i} + \xi_5 \hat{j} + \xi_6 \hat{k} \tag{27}$$

H is the second-order rotation matrix which is expressed as:

$$H = \begin{bmatrix} -\frac{1}{2}(\xi_5^2 + \xi_6^2) & 0 & 0 \\ \xi_4\xi_5 & -\frac{1}{2}(\xi_4^2 + \xi_6^2) & 0 \\ \xi_4\xi_6 & \xi_5\xi_6 & -\frac{1}{2}(\xi_4^2 + \xi_5^2) \end{bmatrix} \tag{28}$$

The equations for both force (23) and moment (24), are confined up to the second order of wave slope (ϵ^2) to calculate the second-order force and moment acting over the body surface. These are expressed as the following equation:

$$\begin{aligned} F^{(2)} = &\int_{S_0} p^{(0)} (H\hat{n}')\, dS + \int_{S_0} p^{(1)} (\theta^{(1)} \times \hat{n}') dS + \\ &\int_{S_0} p^{(2)} \hat{n}' dS + \underbrace{\int_s \zeta_r^{(1)} p^{(0)} (\theta^{(1)} \times \hat{n}') ds}_{= 0 \text{ when } p^{(0)} = 0 \text{ on } s} + \\ &\int_s \zeta_r^{(1)} p^{(1)} \hat{n}' ds + \underbrace{\int_s \zeta_r^{(2)} p^{(2)} \hat{n}' ds}_{= 0 \text{ when } p^{(0)} = 0 \text{ on } s} \end{aligned} \tag{29}$$

$$
\begin{aligned}
M^{(2)} = & \int_{S_0} p^{(0)} \left[H(x' \times n') + \xi^{(1)} \times (\theta^{(1)} \times n') \right] dS + \\
& \int_{S_0} p^{(1)} \left[\xi^{(1)} \times \hat{n}' + \theta^{(1)} \times (x' \times n') \right] dS + \\
& \int_{S_0} p^{(2)} (x' \times n') dS + \\
& \underbrace{\int_{s} \zeta_r^{(1)} p^{(0)} \left[\xi^{(1)} \times n' + \theta^{(1)} \times (x' \times n') \right] ds +}_{= 0 \text{ when } p^{(0)} = 0 \text{ on } s} \\
& \int_{s} \zeta_r^{(1)} p^{(1)} (x' \times n') ds + \underbrace{\int_{s} \zeta_r^{(2)} p^{(0)} (x' \times n') ds}_{= 0 \text{ when } p^{(0)} = 0 \text{ on } s}
\end{aligned} \tag{30}
$$

The interaction of bi-chromatic waves, representing regular waves, results in the emergence of forces and moments at both sum and difference frequencies. The application of perturbation theory as mentioned in subsection 2.3, is used to calculate the second-order force and moment that consider the interaction between two wave trains characterized by varying amplitudes and frequencies.

The total second-order wave drift forces and moments are shown in equations (29) and (30), which are used to calculate the cumulative effects of forces and moments from the both sum and difference frequency, as outlined below.

$$F^{(2)}(\omega_m, \omega_n) = F^{(2d)}(\omega_m, \omega_n) + F^{(2s)}(\omega_m, \omega_n) \tag{31}$$

$$M^{(2)}(\omega_m, \omega_n) = M^{(2d)}(\omega_m, \omega_n) + M^{(2s)}(\omega_m, \omega_n) \tag{32}$$

Where,

- $F^{(2s)}(\omega_m, \omega_n)$ is the sum frequency component of the total second-order force.
- $F^{(2d)}(\omega_m, \omega_n)$ is the difference frequency component of the total second-order force.
- $M^{(2s)}(\omega_m, \omega_n)$ is the sum frequency component of the total second-order moment.
- $M^{(2d)}(\omega_m, \omega_n)$ is the difference frequency component of the total second-order moment.

When considering a bi-chromatic wave composed of two regular wave trains, each characterized by its respective frequencies and amplitudes, denoted as ω_m, ω_n, Am, and An. A pair of bi-chromatic wave frequencies difference is shown in Figure 4. Which is referred from [2].

A series of second-order transfer functions play an important role in explaining the complex interaction between Am and An amplitudes giving insight into the generation of sum frequency and difference frequency components within the wave system. These transfer functions are commonly referred to as quadratic transfer functions (QTFs).

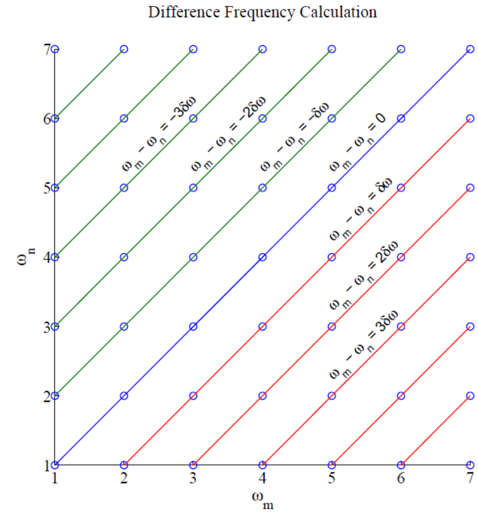

FIGURE 4: PAIR OF DIFFERENCE FREQUENCIES WITHIN THE BI-FREQUENCY PLANE (ω_m, ω_n)

$$Q_i^{(2d)}(\omega_m, \omega_n) = \frac{F_i^{(2d)}(\omega_m, \omega_n)}{A_m A_n} \quad for\, i = 1, 2, 3 \tag{33}$$

$$Q_i^{(2d)}(\omega_m, \omega_n) = \frac{M_{i-3}^{(2d)}(\omega_m, \omega_n)}{A_m A_n} \quad for\, i = 4, 5, 6 \tag{34}$$

$$Q_i^{(2s)}(\omega_m, \omega_n) = \frac{F_i^{(2s)}(\omega_m, \omega_n)}{A_m A_n} \quad for\, i = 1, 2, 3 \tag{35}$$

$$Q_i^{(2s)}(\omega_m, \omega_n) = \frac{M_{i-3}^{(2s)}(\omega_m, \omega_n)}{A_m A_n} \quad for\, i = 4, 5, 6 \tag{36}$$

4. HYDRA - NUMERICAL SIMULATION TOOL

The in-house simulation program HydRA is a cutting-edge development founded on the principles of potential theory and the 3D Green function panel method code. This program plays a pivotal role in the comprehensive analysis of wave loads affecting a diverse range of maritime structures, including floating bodies, moored structures, and ships, and taking into account all six degrees of motion.

The HydRA program is capable of operating in both the frequency and time domains, employing a Near-field method. The primary objective of this study is to showcase how HydRA can precisely calculate the intricate motion and force characteristics of different vessels. This study focuses on the calculation of second-order wave drift forces and moments acting on the vessels at both zero speed and forward speed within the dynamic presence of regular waves. This research emphasizes the precision of HydRA as a valuable asset in maritime simulation, promising advancements in understanding and predicting floating structures or vessel behavior under varying wave conditions.

The driving force behind the development of the HydRA program tool is its capability to analyze a variety of fluid-structure interaction scenarios, including responses of floating bodies, seakeeping motions of vessels, offshore and moored structures, as well as second-order wave drift forces acting on bodies. Particularly, the program's evolution has been focused on facilitating analysis of multi-body or vessel responses simultaneously, ship-ship interactions, and mooring line systems for offshore structures. A notable advantage of the HydRA program lies in its adaptability; its in-house development allows for flexible improvements in the coding and enhancement changes in the specific analytical needs, these features not readily available in other software tools.

A brief step-by-step procedure for using this simulation tool is explained as follows: There are two files required to use this numerical tool such as a GDF file and an input file. The geometry of the floating structures or ship hull is discretized into n-numbers of panels as a GDF file. This GDF file has three dimensional each underwater panel's coordinates from the origin of the body. The input file specifies the location of the body in the global fixed coordinate frame, the location of the center of gravity, the mode of vessel motions, the simulation period, and regular wave parameters like height, period, direction, and so on. Upon receiving the input, the program initiates the computation of the frequency-independent segment of the influence matrix. Subsequently, it proceeds to calculate the frequency-dependent components of the influence matrix. Once the influence matrices are fully computed, the program determines source strengths and potentials by solving a linear system of equations derived from the application of Green's identity. Finally, utilizing superimposed velocity potentials, the tool calculates added mass, radiation damping, scattering forces, Response Amplitude Operators (RAOs), added resistance, mean second-order wave drift forces, and so forth.

In time domain analysis, the obtained results from the frequency domain results serve as inputs for calculating the forces and motion of the structures in a rapid time. The specialty of this simulation tool is capable of calculating a more number of vessel motions at the same time. The HydRA software has been developing HydRA-WebSim for a more visual understanding of the fluid-structure interaction which is shown in Figure 5. This web-based maritime simulation builds further on the visualization routines provided by Henrique M. Gaspar [22].

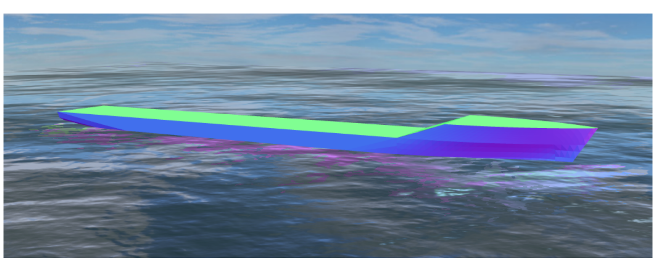

FIGURE 5: HYDRA WEB SIMULATION FOR KCS HULL

The HydRA solutions have been tested and validated against existing commercial and research programs. The HydRA program used simulations have been emerging in a recent study, Sridhar et al. [23] experimentally studied the hydrodynamic response analysis of the FPSO structure for both ballast and fully-loaded conditions. The obtained numerical results from the commercial software Ansys Aqwa, Wamit, and HydRA program were validated against the experimental outcomes.

4.1 Full-scale KCS hull setup

The research benchmark vessel Korea Research Institute of Ships and Ocean Engineering (KRISO) Container Ship (KCS) was chosen for this study. The Full-scaled KCS ship main principle particular is shown in Table 1.

The hull geometry and specifications for this vessel were sourced from the SIMMAN 2008 website, specifically the KCS Geometry. Subsequently, the 3-D modeling software Rhinoceros was used to modify the geometry of the structure as quadrilateral mesh hull forms saved as GDF files. Figure 6 illustrates the underwater mesh panels of the full-scaled KCS hull, comprising a total of 1720 panels.

TABLE 1: KCS MAIN PRINCIPAL PARTICULARS

Main Particulars	Value
Length between water level L_{wl} (m)	232.5
Length between perpendiculars L_{PP} (m)	230
Breadth B (m)	32.2
Depth D (m)	19.0
Draft d (m)	10.8
Displacement ∇ (m^3)	52030
Block coefficient C_b	0.651
Radius of yaw gyration R_{zz}/L_{PP}	0.25
Metacentric height GM (m)	1.20
Vertical center of gravity (From Draft) VCG (m)	3.552
Center of gravity (From Keel) KG (m)	7.248
LCB (% of L from midship, forward +ve)	-1.48%
Froude number (Based on Lpp) F_n	0.26

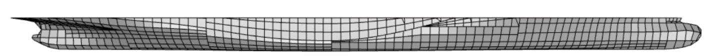

FIGURE 6: KCS HULL UNDERWATER MESH PANELS

FIGURE 7: KCS HULL UNDERWATER FINE MESH PANELS

The selection of the largest panel size was determined by considering $1/8^{th}$ of the shortest wavelength, ensuring that eight panels are encompassed within a single wavelength. Validation of the HydRA program tool was conducted against the finer mesh panels of the KCS underwater configuration, comprising a total of 3346 panels. The RAO results match very well for both cases, a detailed comparison of the results is presented in section 5.

4.2 Methodology

This study aims to enhance the computation of second-order wave drift force and moments specifically for a zero-speed scenario. The methodology involves a numerical analysis of wave drift forces acting on the vessel and its motion in all six degrees of freedom, employing program simulation tools. The HydRA simulation tool calculated the second-order wave drift forces, providing insights into the KCS vessel's response to waves. Additionally, other simulation tools based on 3D-potential flow theory are employed to capture the full-scale responses of the KCS ship. The obtained results from HydRA are validated against the MDLHydroD and WAMIT programs to ensure accuracy and reliability.

5. RESULTS AND DISCUSSIONS

The KCS vessel's mean drift force in surge, under an incident wave direction of $\beta = 240°$ at zero speed, is validated using HydRA simulation results, compared against the MDLHydroD and WAMIT programs is shown in Figure 8. The figure illustrates that the surge drift force results from the HydRA simulation are a good match with the other program results. Particularly in the low wave frequency range ($\omega = 0.03 - 0.4\ rad/s$), the vessel motion is minimal due to the relative wave elevation being small. This leads to a nearly negligible surge drift in this frequency region. Notably, a downward sudden small sharp is observed in between the ($\omega = 0.21 - 0.27\ rad/s$) due to the irregular wave frequency.

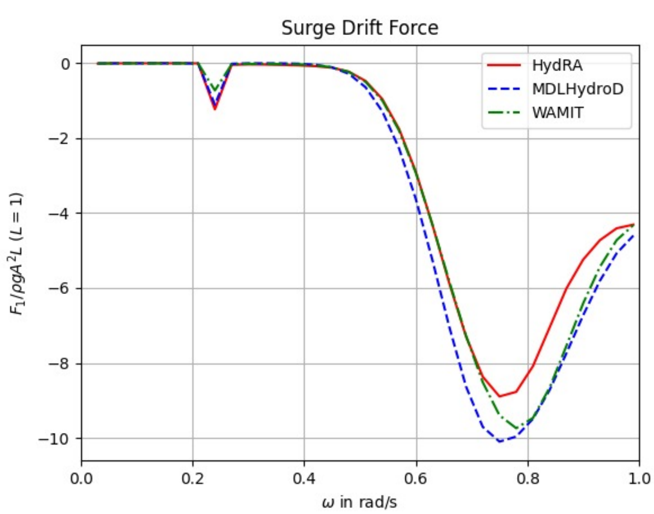

FIGURE 8: MEAN WAVE DRIFT FORCE IN SURGE FOR AT $\beta = 240°$

A notable correlation between wave elevation and the corresponding forces exerted by the waves is seen in the figure. Particularly within the wave frequency range of $\omega = 0.52-0.72\ rad/s$, a significant amplification in motion is primarily attributable to resonance and heightened relative wave elevation. Consequently, the surge drift force experiences a substantial augmentation, reaching at its peak value at $\omega = 0.7231\ rad/s$. However, a distinct deviation emerges between the HydRA results and alternative numerical findings for $\omega > 0.7231\ rad/s$. Within this frequency spectrum, there is an observable gradual decline in the surge mean drift force.

The wave drift force for pitch under a wave direction of $\beta = 150°$ at zero-speed is shown in Figure 9. In the low-frequency region, the sudden peak is raised due to the presence of the irregular wave frequency. As the relative wave heights increase, the pitch drift forces steadily ascend, reaching their zenith at $\omega = 0.52\ rad/s$ Subsequently, the peak gradually diminishes in the higher wave frequency range due to decreased wave heights. Notably, the validated results from the HydRA tool exhibit excellent agreement with those from other program tools.

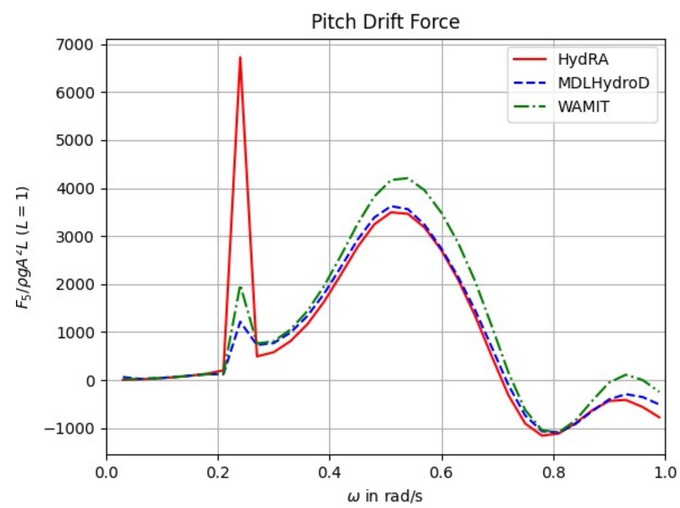

FIGURE 9: MEAN WAVE DRIFT FORCE IN PITCH FOR AT $\beta = 150°$

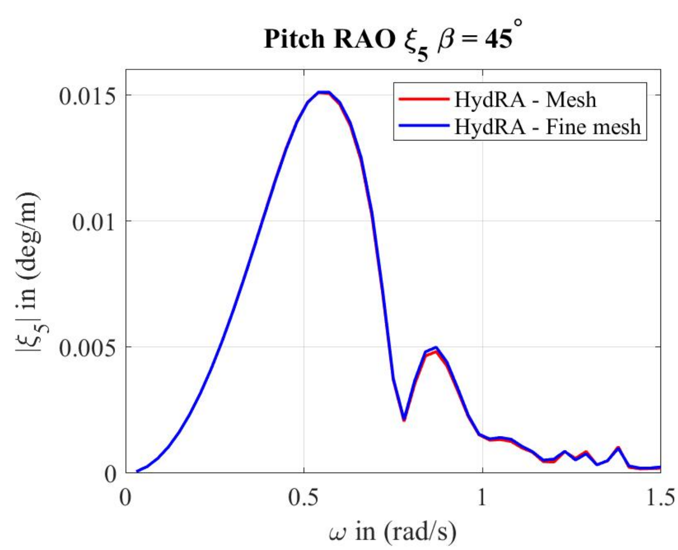

FIGURE 10: PITCH RAO COMPARISON FOR MESH AND FINE MESH FOR $\beta = 45°$

The successful analysis of Response Amplitude Operator (RAO) comparisons between the mesh and fine mesh configurations for the KCS within the HydRA program. This comparison encompasses various modes of motion across different wave directions, as depicted in the accompanying figures. Notably, the fine mesh utilized in the analysis comprises nearly twice the number of underwater panels compared to the mesh configuration selected for this study.

The visual representation provided in the Figure 10, Figure 11 and Figure 12 illustrates a strong alignment between the RAOs of different modes across varying wave directions for both the mesh and fine mesh scenarios. This observation underscores the HydRA program tool's robust capacity to precisely analyze vessel motion and its responses in all six degrees of freedom.

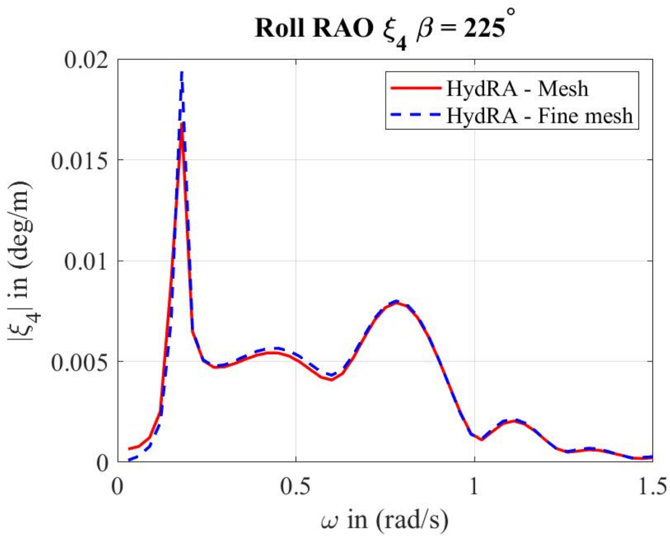

FIGURE 11: ROLL RAO COMPARISON FOR MESH AND FINE MESH FOR β = 225°

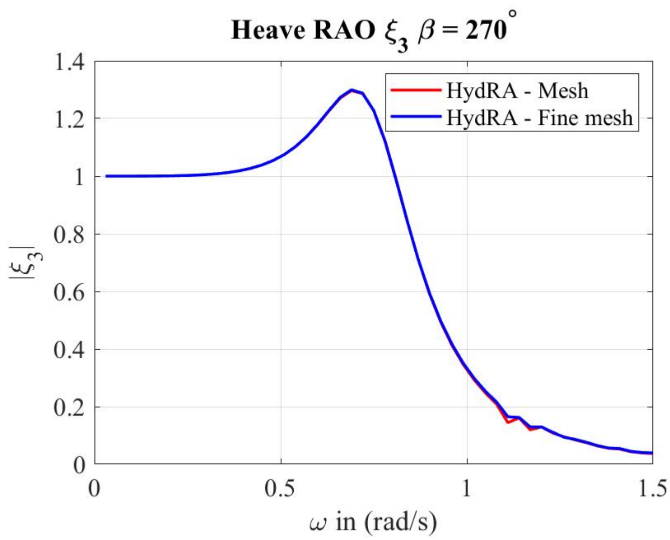

FIGURE 12: HEAVE RAO COMPARISON FOR MESH AND FINE MESH FOR β = 270°

The Pitch Response Amplitude Operator (RAO) of the KCS vessel, considering an incident wave direction of $\beta = 180°$, is validated through the results obtained from HydRA, as depicted in Figure 13. The figure illustrates a strong agreement between the simulated pitch response amplitude operator ξ_5 from HydRA and results obtained from other programs.

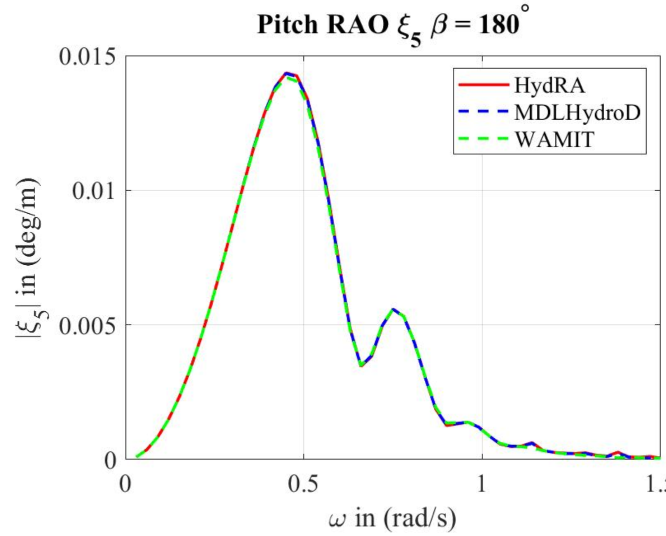

FIGURE 13: PITCH RAO COMPARISON FOR INCIDENT WAVE DIRECTION OF β = 180°

As the wave frequency increases from very low values, the amplitude of the KCS vessel's response experiences rapid growth. It attains maximum response when the wave frequency meets with the vessel's natural frequency. Subsequently, the response peaks start to reduce when $\omega = 0.465\ rad/s$. Notably, the reduction in pitch (RAO) response resumes an upward trend to reach a minor peak at $\omega = 0.75\ rad/s$, after that once again the vessel response decreases toward the higher wave frequency.

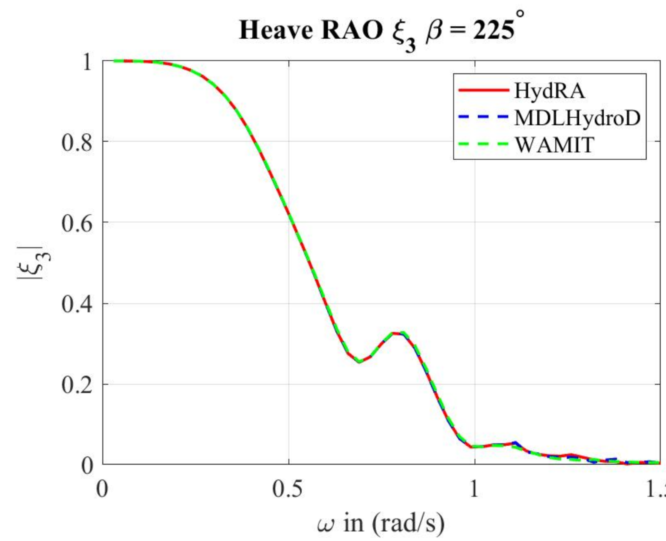

FIGURE 14: HEAVE RAO COMPARISON FOR INCIDENT WAVE DIRECTION OF β = 225°

The Heave RAO (ξ_3) for the KCS vessel is shown in Figure 14, corresponding to an incident wave direction of $\beta = 225°$.

The figure shows that the validated HydRA results closely match with the WAMIT and MDLHydroD programs.

In this RAO, a peak is observed at lower wave frequencies, indicative of the vessel's maximal response within this frequency range. Subsequently, the maximum response gradually diminishes until $\omega = 0.69\ rad/s$. A minor peak appears at $\omega = 0.8\ rad/s$, followed by a gradual decrease in the heave RAO as wave frequencies continue to increase.

The validation of roll RAO ξ_4 HydRA results against other programs for the KCS vessel under an incident wave direction of $\beta = 135°$ is shown in Figure 15.

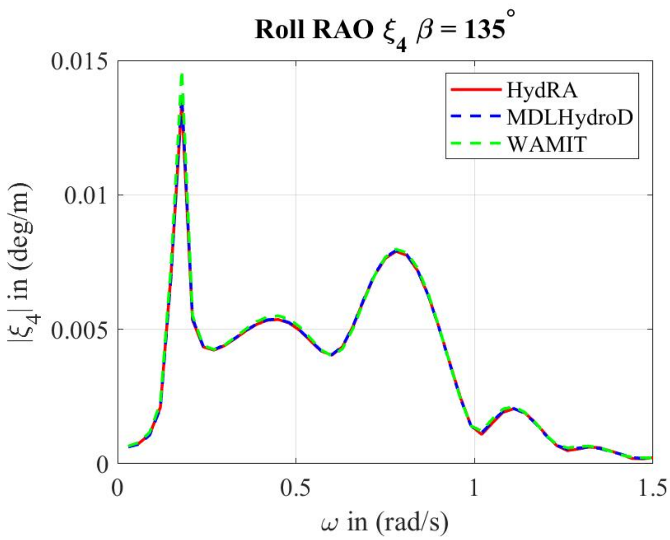

FIGURE 15: ROLL RAO COMPARISON FOR INCIDENT WAVE DIRECTION OF $\beta = 135°$

This figure illustrates a maximum peak occurring in the low wave frequency region at $\omega = 0.18\ rad/s$. followed by a sudden decrease until $\omega = 0.24\ rad/s$. Subsequently, consecutive peaks emerge across the wave frequency spectrum. Notably, a significant peak is observed at $\omega = 0.78\ rad/s$. These findings suggest that the amplitude of the vessel's roll motion fluctuates over different frequency ranges, indicating significant roll motion experienced by the ship under bow sea conditions ($\beta = 135°$).

6. CONCLUSION

This study has successfully integrated second-order wave drift forces into the HydRA program tool as part of its hydrodynamic responses analysis. The analysis included evaluating the second-order mean wave drift force at $\beta = 240°$, as well as examining the pitch, heave, and roll Response Amplitude Operator (RAO) for the Full-scale KRISO Container Ship (KCS) under various incident wave directions such as $\beta = 180°$, $\beta = 225°$, and $\beta = 135°$. Validation was performed by comparing the HydRA simulation results with those obtained from the MDLHydroD and WAMIT programs, demonstrating a robust agreement with these alternative programs.

Furthermore, the study underscores the HydRA program's expertise as a 3D Green function panel method code simulation tool. This tool exhibits notable capabilities in conducting hydrodynamic analyses for offshore structures, vessels, or any floating bodies within wave conditions. Notably, The development of calculating second-order wave drift force for forward speed is underway within the HydRA tool. Future research will specifically concentrate on capturing the mean wave drift for a vessel at forward speed.

7. ACKNOWLEDGMENTS

The authors thanks to Dr.Amitava Guha for sharing his panel method code-based simulation tool "MDLHydroD" for the calculation of wave drift forces and moments at both zero speed and forward speed.

The authors also would like to thank Prof. Henrique Murilo Gaspar for the development of the "Vessels.js" structure being made possible.

REFERENCES

[1] Fonseca, Nuno, Pessoa, Joa o and Guedes Soares, Carlos. "Calculation of second order drift forces on a FLNG accounting for difference frequency components." *International Conference on Offshore Mechanics and Arctic Engineering*, Vol. 48234: pp. 369–377. 2008.

[2] Somayajula, Abhilash and Falzarano, Jeffrey. "A comparative assessment of approximate methods to simulate second order roll motion of FPSOs." *Ocean Systems Engineering* Vol. 7 No. 1 (2017): pp. 53–74.

[3] Huijsmans, RH and Hermans, AJ. "The effect of the steady perturbation potential on the motions of a ship sailing in random seas." *International Conference on Numerical Ship Hydrodynamics, 5th*. 1988.

[4] Remery, GFM and Hermans, AJ. "The slow drift oscillations of a moored object in random seas." *Society of Petroleum Engineers Journal* Vol. 12 No. 03 (1972): pp. 191–198.

[5] Hermans, Aad J and Sierevogel, Lisette M. "A discussion on the second-order wave forces and wave drift damping." *Applied ocean research* Vol. 18 No. 5 (1996): pp. 257–263.

[6] Pinkster, Jo A and Hooft, JP. "Low frequency second order wave forces on vessels moored at sea." *11th Symposium on Naval Hydrodynamics, ONR, London, England, 1976*. 1976.

[7] Pinkster, Johannes Albert. "Low frequency second order wave exciting forces on floating structures." (1980).

[8] Maruo, H. "The drift of a Body floating on waves." *Journal of Ship Research* Vol. 4 No. 1 (1978): pp. 2–15.

[9] Papanikolaou, Apostolos. "On integral-equation-methods for the evaluation of motions and loads of arbitrary bodies in waves." *Ingenieur-Archiv* Vol. 55 No. 1 (1985): pp. 17–29.

[10] Papanikolaou, A and Zaraphonitis, G. "Improved Method for the Evaluation of Second-Order Motions and Loads of 3D Floating Bodies in Waves." (1987).

[11] Liu, Shukui, Papanikolaou, Apostolos and Zaraphonitis, George. "Prediction of added resistance of ships in waves." *Ocean Engineering* Vol. 38 No. 4 (2011): pp. 641–650.

[12] Guha, Amitava and Falzarano, Jeffrey. "Estimation of hydrodynamic forces and motion of ships with steady forward

speed." *International Shipbuilding Progress* Vol. 62 No. 3-4 (2015): pp. 113–138.

[13] Yasukawa, Hironori, Hirata, Noritaka, Matsumoto, Akinori, Kuroiwa, Ryota and Mizokami, Shuji. "Evaluations of wave-induced steady forces and turning motion of a full hull ship in waves." *Journal of marine science and technology* Vol. 24 (2019): pp. 1–15.

[14] Fournarakis, Nikos, Papanikolaou, Apostolos and Liu, Shukui. "Estimation of the drift forces and added resistance in waves of the KVLCC2 tanker." *Journal of Ocean Engineering and Marine Energy* Vol. 3 (2017): pp. 139–149.

[15] Guha, Amitava. "Development of a computer program for three dimensional frequency domain analysis of zero speed first order wave body interaction." Ph.D. Thesis, Texas A & M University. 2013.

[16] Guha, Amitava. "Development and application of a potential flow computer program: determining first and second order wave forces at zero and forward speed in deep and intermediate water depth." Ph.D. Thesis. 2016.

[17] Somayajula, Abhilash and Falzarano, Jeffrey. "Large-amplitude time-domain simulation tool for marine and offshore motion prediction: Ergodicity study of coupled parametric roll motion in irregular seas." *Marine Systems & Ocean Technology* Vol. 10 (2015): pp. 1–17.

[18] Jose, Alwin, Falzarano, Jeffrey and Wang, Hao. "Development of Coupled Program Fast-Simdyn and Study of Non-Linear Hydrodynamics, Coupled With Negative Damping and Aerodynamics of Floating Offshore Wind Turbines." *Journal of Offshore Mechanics and Arctic Engineering* Vol. 142 No. 2 (2020): p. 021904.

[19] Guha, Amitava, Somayajula, Abhilash and Falzarano, Jeffrey. "Time domain simulation of large amplitude motions in shallow water." *SNAME Offshore Symposium*: p. D013S010R007. 2016. SNAME.

[20] Ramachandran, Krishnavelu, Borsutkar, Visharad and Somayajula, Abhilash Sharma. "Comparison Between Experiments and Simulations for a Ship Maneuvering in Waves." *International Conference on Offshore Mechanics and Arctic Engineering*, Vol. 86878: p. V005T06A044. 2023. American Society of Mechanical Engineers.

[21] Edition, First, Journée, JMJ and Massie, WW. "Offshore hydromechanics." *Delft University of Technology* (2001).

[22] Gaspar, Henrique. "Current State of the Vessel. JS Library: A Web-Based Toolbox for Maritime Simulations." *SNAME International Marine Design Conference*: p. D031S007R003. 2022. SNAME.

[23] Sridhar, K, Sannasiraj, SA and Sundaravadivelu, R. "Hydrodynamic Response Analysis of Ultra-Deep Water FPSO System Using Ansys Aqwa, Wamit, and HydRA." *International Conference on Offshore Mechanics and Arctic Engineering*, Vol. 86878: p. V005T06A041. 2023. American Society of Mechanical Engineers.